Electronic Supplementary Material (ESI) for Energy & Environmental Science.
This journal is © The Royal Society of Chemistry 2020

Supporting Information

Shallow-Layer Pillaring of Conductive Polymer in Monolithic Grains to Drive Superior Zinc Storage *via* Cascading Effect

Zhenguo Yao[a,b], Qingping Wu[a], Keyi Chen[a,b], Jianjun Liu[a,b] *, Chilin Li[a,b] *

[a] State Key Laboratory of High Performance Ceramics and Superfine Microstructure, Shanghai Institute of Ceramics, Chinese Academy of Sciences, 585 He Shuo Road, Shanghai 201899, China.

Email: chilinli@mail.sic.ac.cn and jliu@mail.sic.ac.cn

[b] Center of Materials Science and Optoelectronics Engineering, University of Chinese Academy of Sciences, Beijing 100049, China.

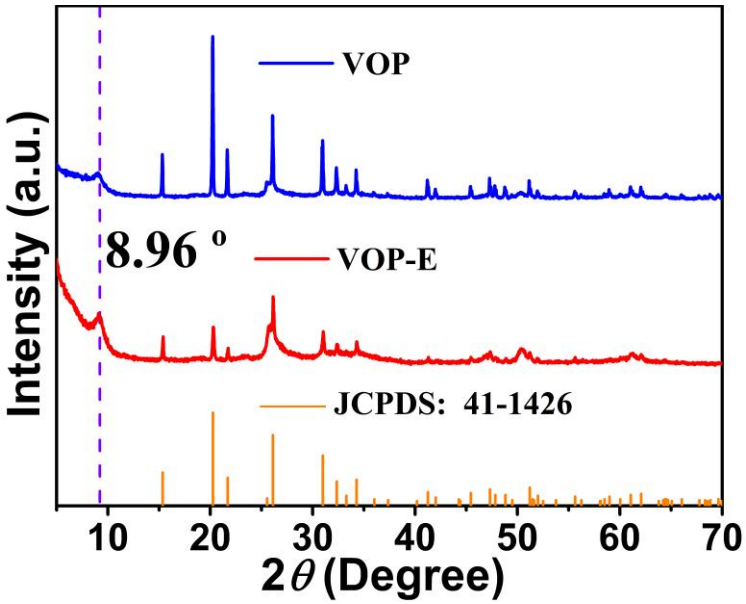

Figure S1. XRD patterns of as-prepared VOP and VOP-E powders.

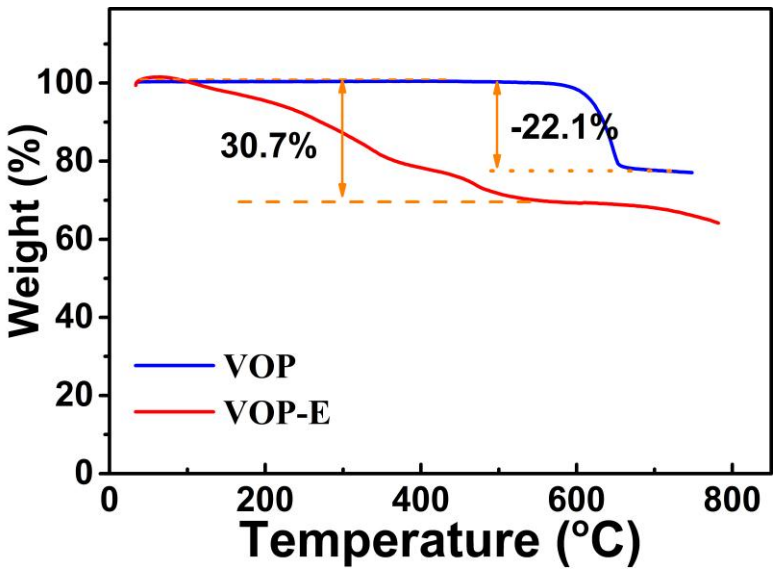

Figure S2. Comparison of TGA curves of as-prepared VOP and VOP-E.

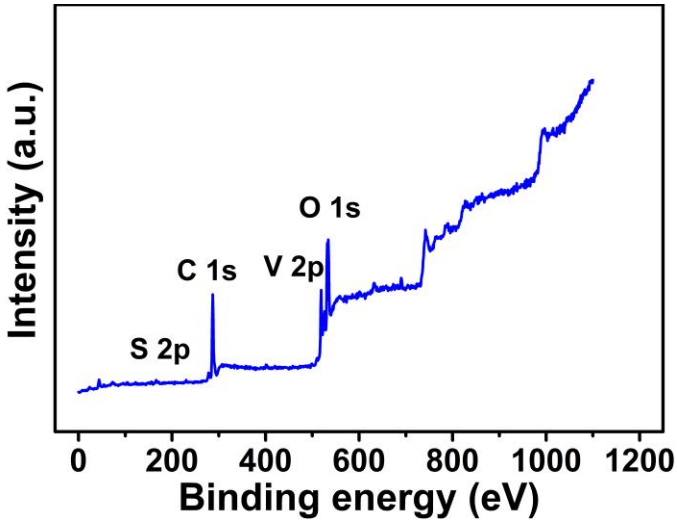

Figure S3. Survey XPS spectrum of pristine VOP.

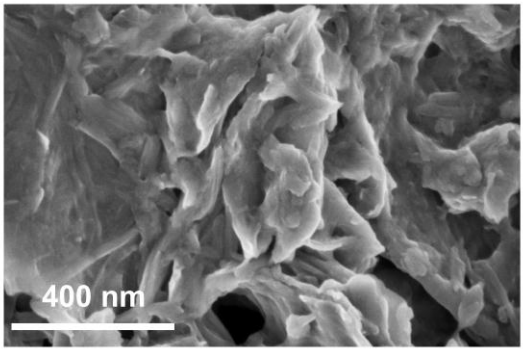

Figure S4. Magnified SEM image of pristine VOP monolithic grain.

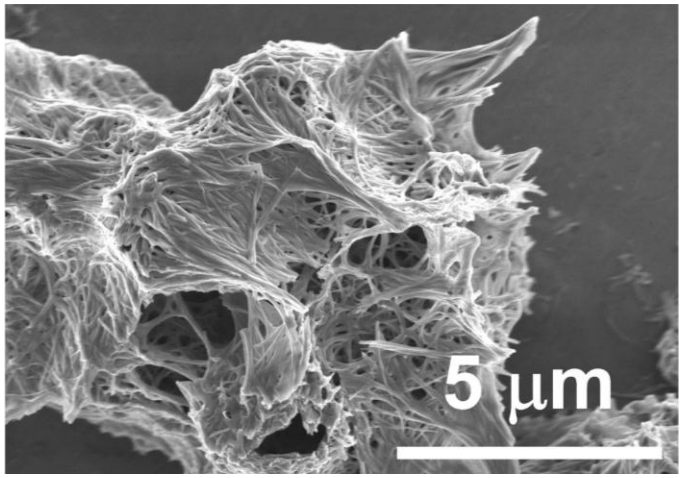

Figure S5. SEM image of VOP-E powder.

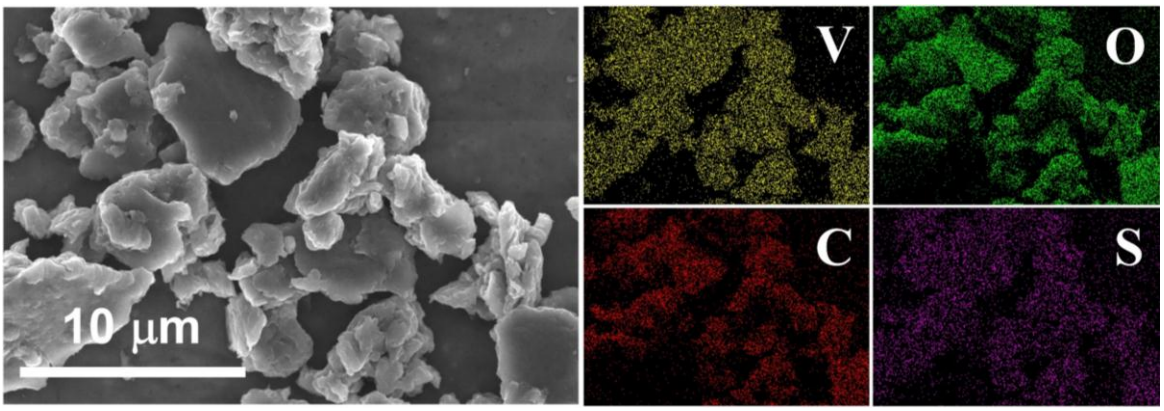

Figure S6. SEM image and corresponding EDS element mapping of pristine VOP.

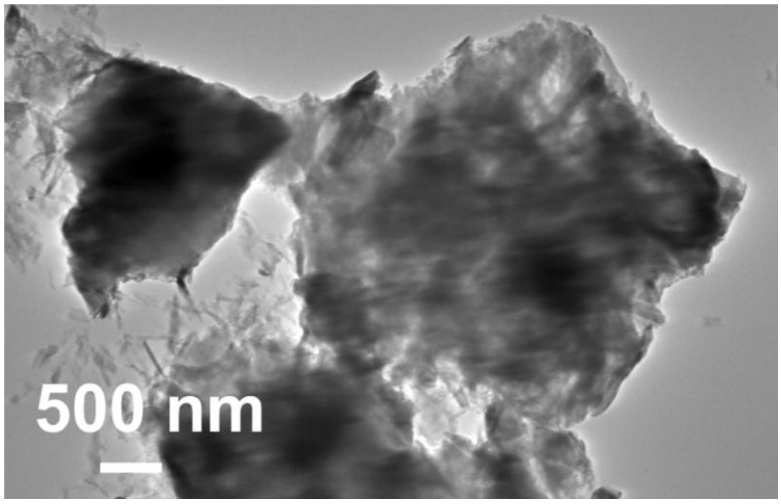

Figure S7. TEM image of pristine VOP.

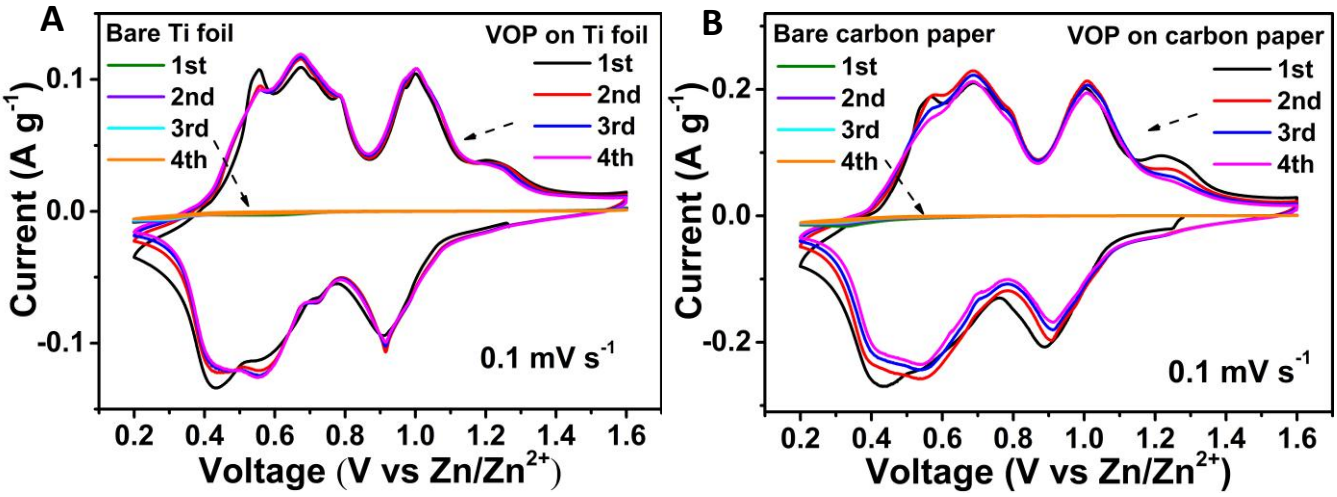

Figure S8. CV curves of VOP electrodes on (**A**) planar Ti foil collector and (**B**) carbon paper at 0.1 mV s^{-1} during the initial four cycles. The CV curves of corresponding current collectors without VOP loading are also displayed as comparisons.

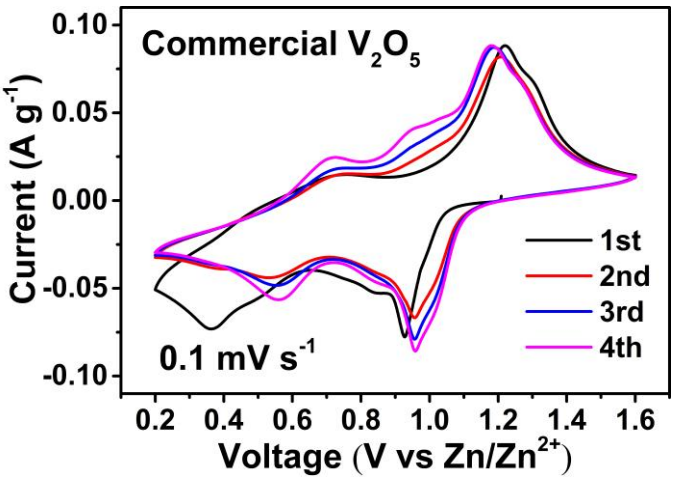

Figure S9. CV curves of commercial V_2O_5 electrode at 0.1 mV s^{-1} during the initial four cycles.

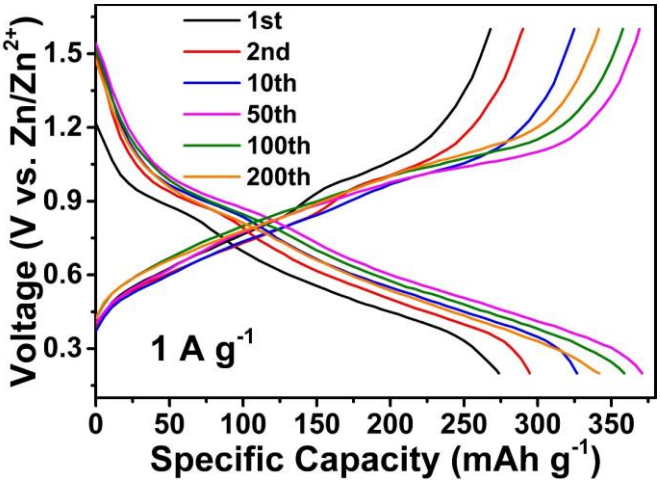

Figure S10. Charge/discharge curves of VOP electrode pasted on Ti foil in different cycling stages at 1.0 A g^{-1}.

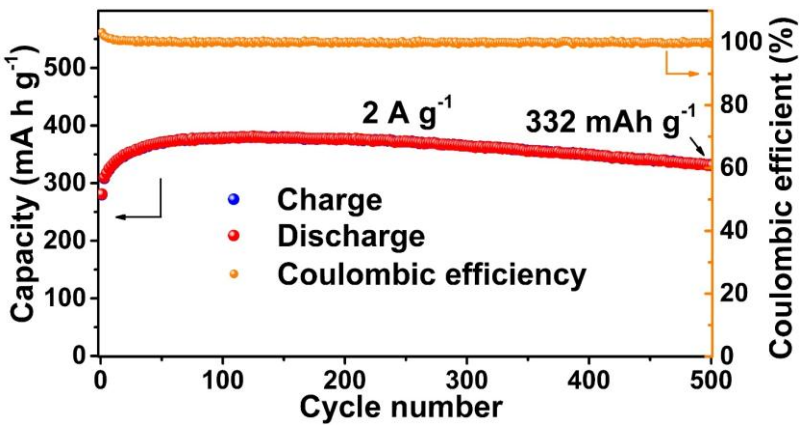

Figure S11. Cycling performance of VOP electrode pasted on Ti foil at 2 A g^{-1}.

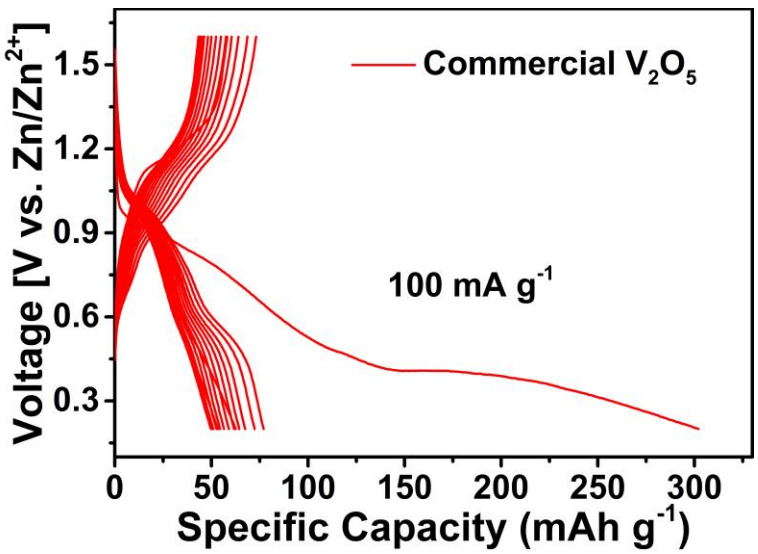

Figure S12. Charge/discharge curves of commercial V_2O_5 electrode at 100 mA g^{-1} during the early cycles.

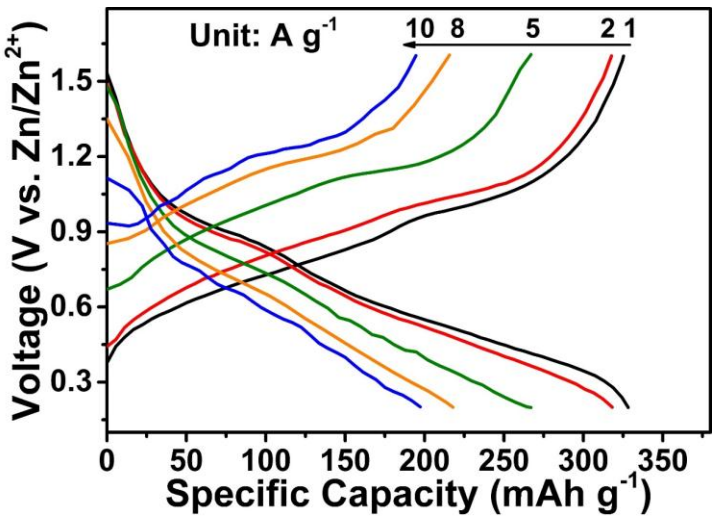

Figure S13. Typical charge-discharge curves of VOP electrode pasted on Ti foil at different current densities.

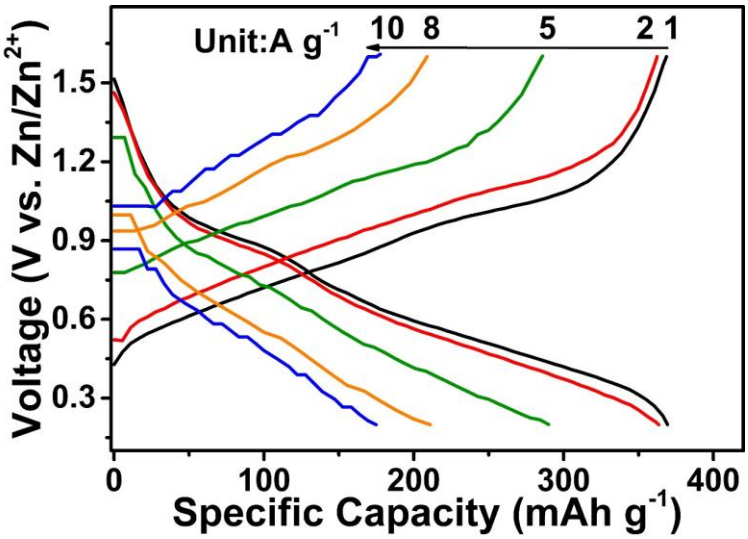

Figure S14. Galvanostatic charge-discharge curves of VOP electrode with excess PEDOT pillaring at different current densities.

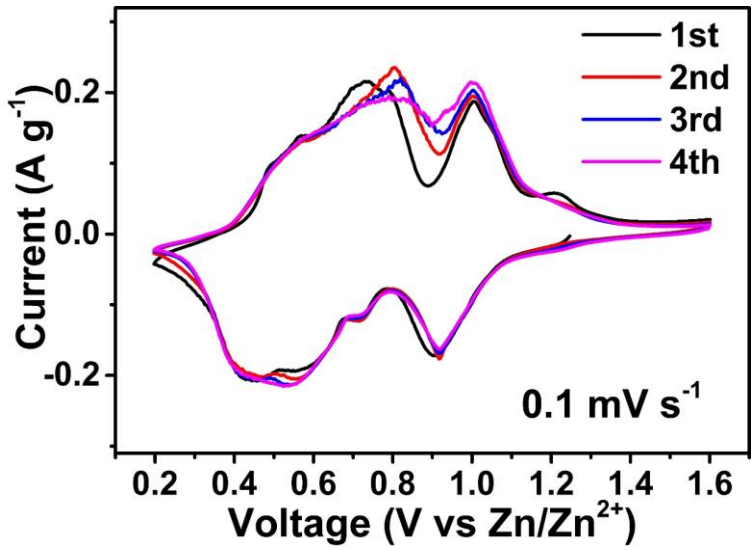

Figure S15. CV curves of VOP electrode with excess pillaring of PEDOT at 0.1 mV s^{-1} during the initial four cycles.

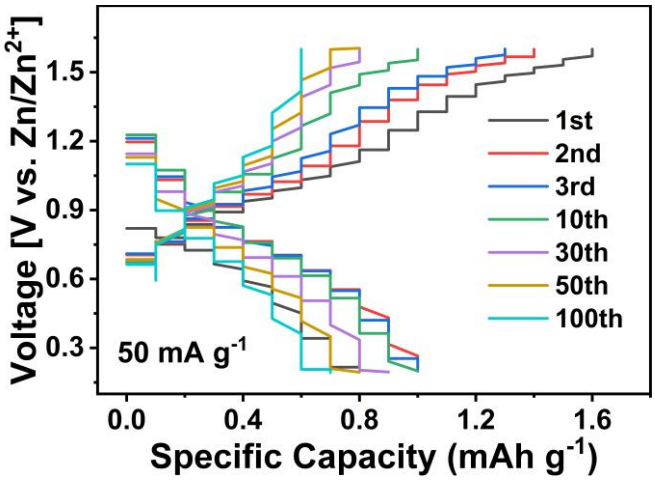

Figure S16. Galvanostatic charge/discharge curves of pure carbon paper electrode at 50 mA g^{-1}. The capacity contribution (<1.5 mAh g^{-1}) of carbon paper current collector is ignorable compared with that of VOP (370 mAh g^{-1} at 1000 mA g^{-1}).

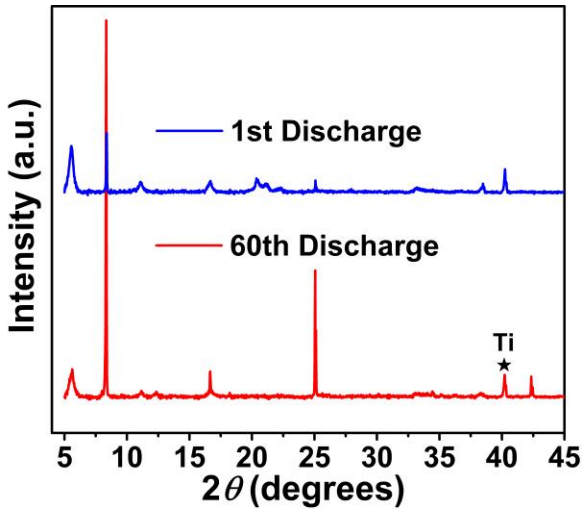

Figure S17. XRD patterns of cycled VOP electrodes at the initial discharged state and at the discharged state after 60 cycles.

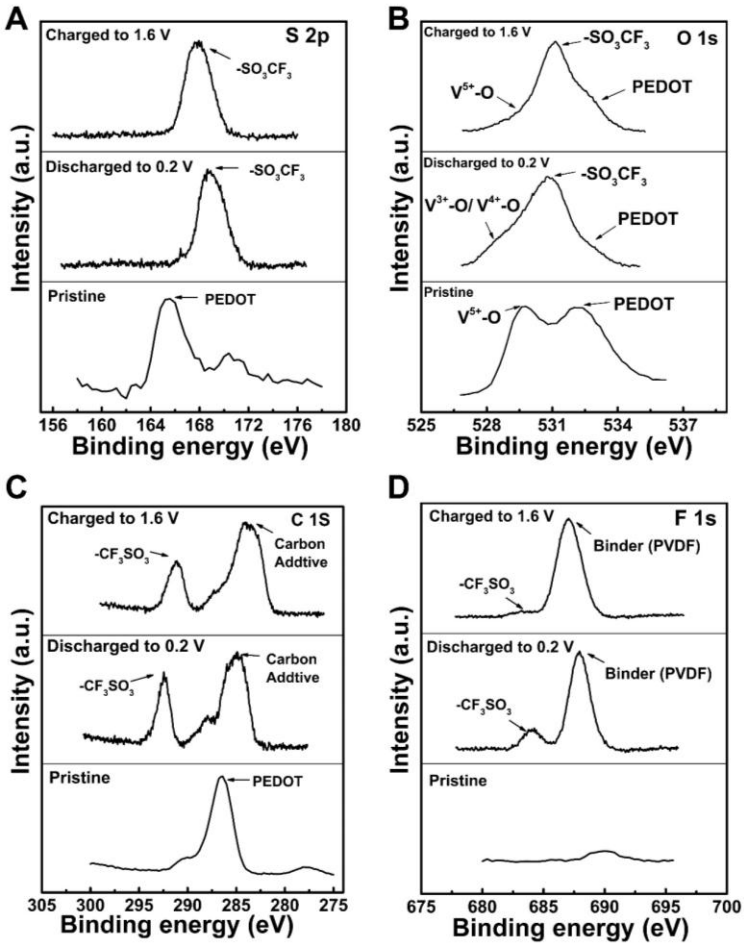

Figure S18. XPS spectra of (**A**) S 2p, (**B**) O 1s, **(C)** C 1s, and (**D**) F 1s regions of VOP electrodes at the initial and fully discharged/charged states.

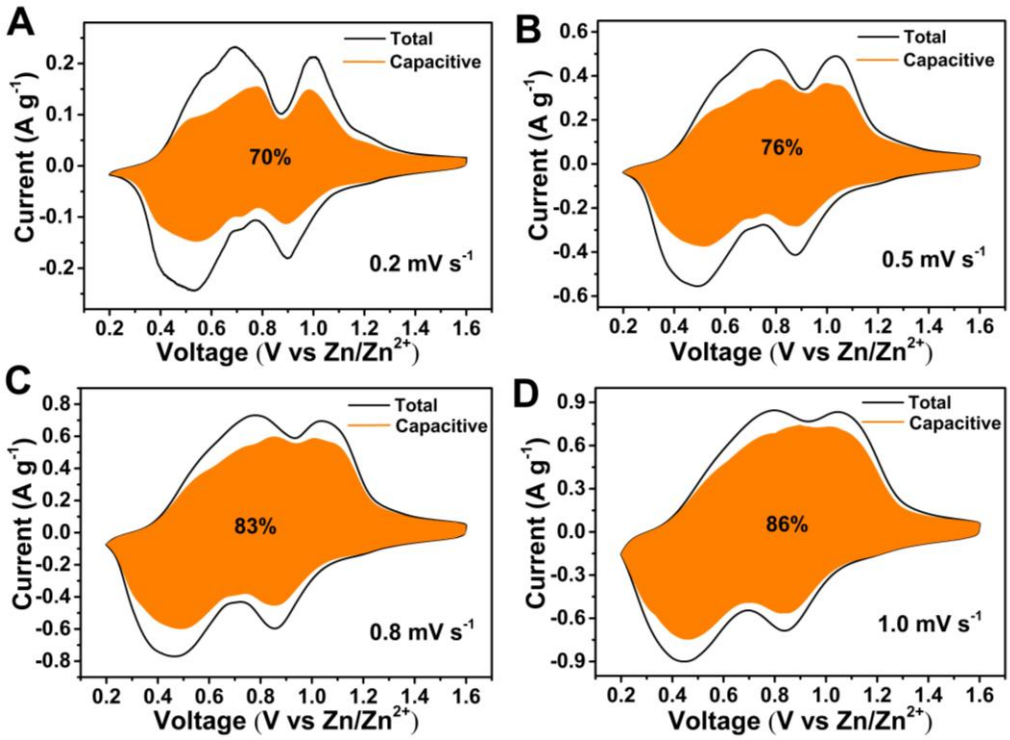

Figure S19. CV curves of VOP electrode with capacitive contribution (orange region) outlined from total current at (**A**) 0.2 mV s^{-1}, (**B**) 0.5 mV s^{-1}, (**C**) 0.8 mV s^{-1}, and (**D**) 1.0 mV s^{-1}.

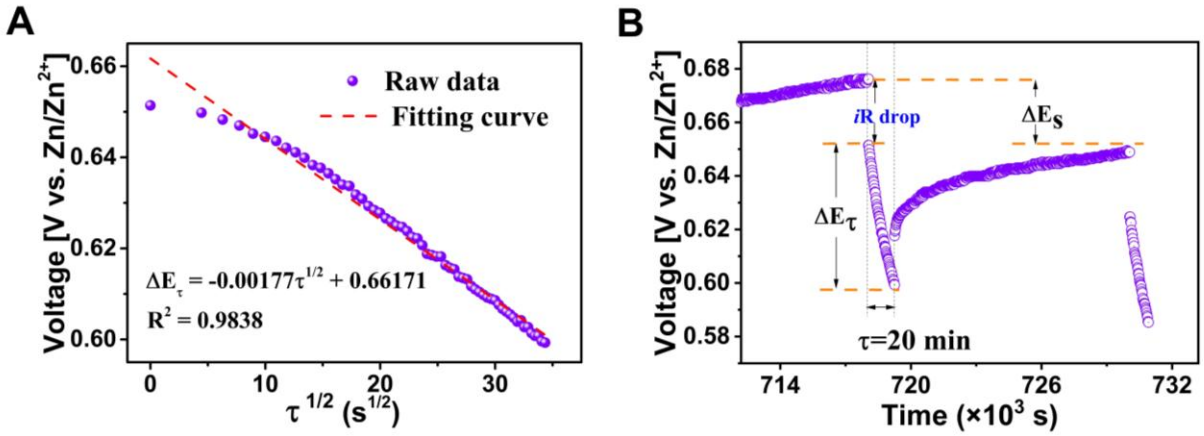

Figure S20. (**A**) Linear relationship fitting between transient cell voltage and the square root of current pulse time in a single-step GITT experiment. (**B**) Schematic illustration of a typical single GITT step during discharging.

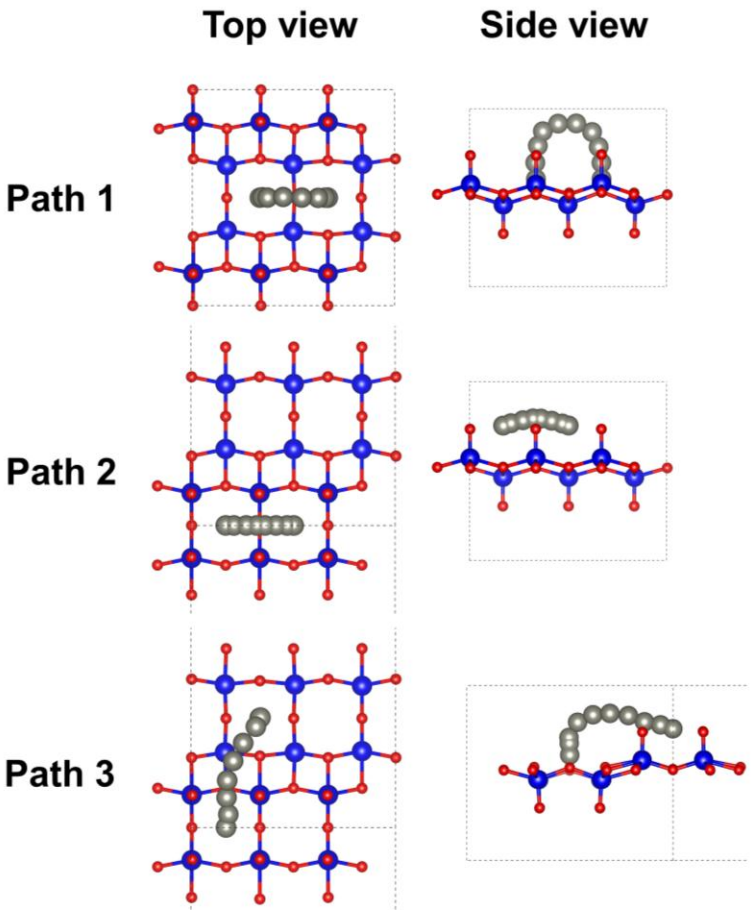

Figure S21. Top and side views of three potential migration paths of Zn in expanded VOP interlayers.

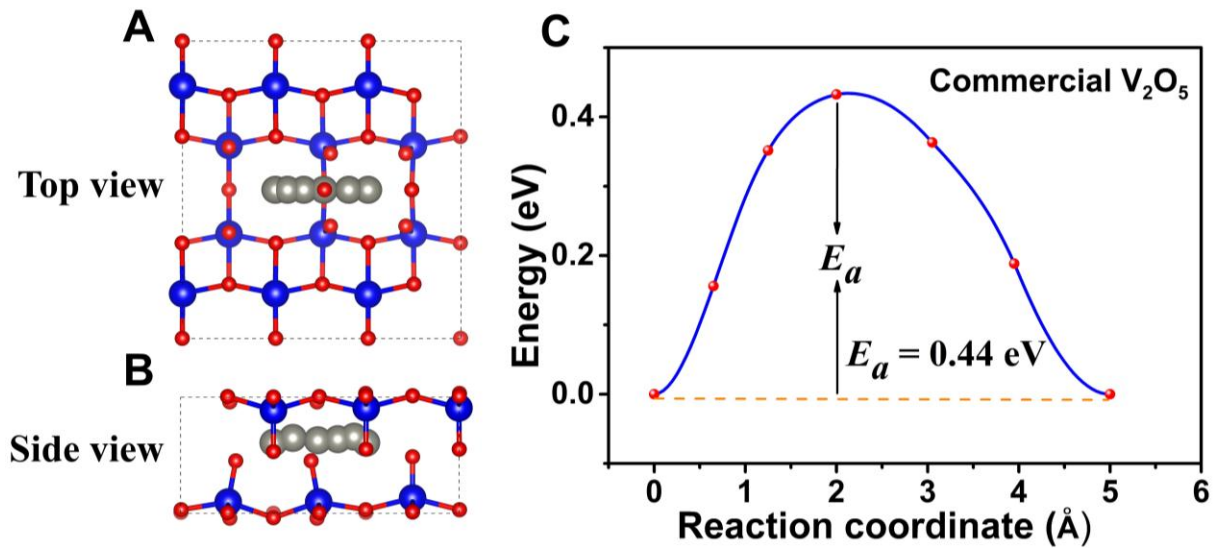

Figure S22. (**A**) Top view, (**B**) side view, and (**C**) diffusion energy barrier profile of Zn^{2+} diffusion in commercial V_2O_5 without interlayer expansion.